

High-Throughput Experimentation in Electrochemistry for Alkaline Water Electrolysis

Inka Dessel, Deniz Dogan, Rüdiger-Albert Eichel, Burkhard Hecker, Christian Hofmann, Florian Huber, Asha Jakob, Hans-Joachim Kost, Patrick Löb, Andreas Müller, Sarifahnurliza Sahehmahamad, Volkmarm M. Schmidt, Fabian Schneider, Hermann Tempel, Guido Wasserschaff* and Athanassios Ziogas

DOI: 10.1002/cite.202300234

 This is an open access article under the terms of the [Creative Commons Attribution](https://creativecommons.org/licenses/by/4.0/) License, which permits use, distribution and reproduction in any medium, provided the original work is properly cited.

High-throughput experimentation, a well-established and powerful tool in the field of heterogeneous catalysis screening, has been extended to the field of electrochemistry. A parallel and modular high-throughput screening platform was designed, involving the development of a new modular electrochemical flow cell by the Fraunhofer Institute for Microengineering and Microsystems (IMM) in cooperation with hte GmbH and IEK-9 / FZ Jülich GmbH. Here, this platform is introduced for alkaline water electrolysis, showing initial results that underline the flexibility, comparability, and accuracy of the experiments.

Keywords: Alkaline water electrolysis, Anion exchange membrane water electrolysis, Electrochemistry, High-throughput experimentation, Modular flow cells

Received: November 30, 2023; revised: April 17, 2024; accepted: April 18, 2024

1 High-Throughput Screening in Electrochemistry

Parallel testing accelerates the development of heterogeneous catalysis compared to classical approaches [1]. High-throughput experimentation means performing an experiment in a setup with multiple reactors in parallel and under identical and reproducible process conditions (T , p , etc.). The use of standardized screening equipment and workflows is indispensable but not established for electrochemical processes [2–4]. Nevertheless, exact and reproducible screening conditions between the different electrochemical flow cells – instead of reactors – arranged in a parallel setup minimize the influences of the test setup and therefore improve the quality of the test data obtained. In cooperation with IEK-9 / FZ Jülich GmbH, a 16-fold high-throughput screening platform for water-based electrolysis reactions was developed and tested under realistic operation conditions in different water electrolysis settings.

2 New Modular Screening Platform for High-Throughput Experimentation in Electrochemistry

The high-throughput screening platform is modular in design and can be freely configured for electrochemical screening operation with up to 16 electrochemical flow cells in parallel (Fig. 1). The flow rate, temperature, and pressure of different fluids and electrolytes can be regulated for the


individual flow cells. An electrolyte management system for automatic preparation, refilling, and disposal can be optionally added, as can possible humidification for gases, for gas diffusion electrode (GDE) applications.


The product streams leaving the flow cells can be divided using gas/liquid separators and the fluids can be circulated or pumped through the flow cell in a single pass. The

¹Inka Dessel, ^{2,3}Deniz Dogan

 <https://orcid.org/0000-0002-1923-7337>,

^{2,3}Prof.-Dr. Rüdiger-Albert Eichel

 <https://orcid.org/0000-0002-0013-6325>, ²Dr. Burkhard Hecker

 <https://orcid.org/0000-0003-0462-901X>, ⁴Christian Hofmann,

¹Dr. Florian Huber, ¹Asha Jakob, ⁴Hans-Joachim Kost,

⁴Dr. Patrick Löb, ¹Dr. Andreas Müller,


^{1,5}Sarifahnurliza Sahehmahamad, ⁵Prof. Dr. Volkmarm M. Schmidt,

¹Dr. Fabian Schneider, ²Dr. Hermann Tempel

 <https://orcid.org/0000-0002-9794-6403>,

¹Guido Wasserschaff (Guido.wasserschaff@hte-company.de),

⁴Dr. Athanassios Ziogas

 <https://orcid.org/0000-0002-9373-8674>

¹hte GmbH, Kurpfalzring 104, 69123 Heidelberg, Germany.

²Forschungszentrum Jülich GmbH, Institute of Energy and Climate Research, Fundamental Electrochemistry (IEK-9), Wilhelm-Johnen-Straße, 52428 Jülich, Germany.

³Institute of Physical Chemistry, RWTH Aachen University, 52074 Aachen, Germany.

⁴Fraunhofer Institute for Microengineering and Microsystems IMM, Carl-Zeiss-Straße 18–20, 55129 Mainz, Germany.

⁵Institut für Chemische Verfahrenstechnik, Hochschule Mannheim, Paul-Wittsack-Straße 10, 68163 Mannheim, Germany.

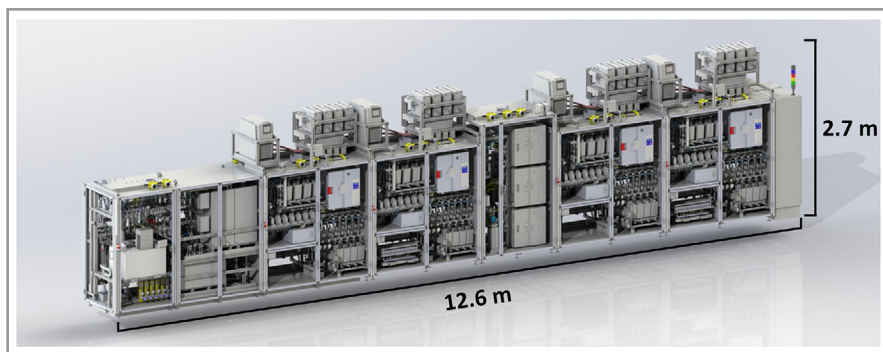


Figure 1. 16-fold high-throughput platform for electrochemistry from hte GmbH.

platform can be operated 24/7 and may be equipped with analytic systems for online analysis (e.g., gas chromatography). An autosampler for offline analysis of liquid samples, e.g., can also be integrated.

The high-throughput platform for electrochemistry also contains a new package for electrochemical analytics in the experiment control suite (hteControl4TM), which is used to edit experiment jobs and for job scheduling. hteControl4TM sends process trend data and electrochemical analysis data to the myhte4TM proprietary database for data evaluation [5] and fast visualization of electrochemical impedance or current voltage diagrams, for instance. The new software extension allows automated feedback loops and process

parameter adjustment of Metrohm potentiostats via their integrated NOVA[®] suite software package.

3 New Modular Flow Cells for Electrochemistry

The flow cell design for electrochemical applications in electrolysis must be robust to allow reproducible measurements. The design must also streamline handling and cleaning procedures to reduce flow cell preparation time. Furthermore, a certain degree of flexibility regarding

usability for different electrochemical applications is an advantage and reduces initial investment cost [6–9].

As such, the Fraunhofer Institute for Microengineering and Microsystems (IMM) developed a new modularized flow cell construction kit with the collaboration of hte GmbH and IEK-9 / FZ Jülich GmbH.

The flow cell construction kit consists of various parts. The housing is made of polyether ether ketone (PEEK; Fig. 2a) and the exchangeable current collector is made of titanium. The active temperable flow cell is designed for an operation window of 20–90 °C and <5 barg and will be designed for up to 60 barg in a future version. The gap between the electrodes and the membrane/diaphragm

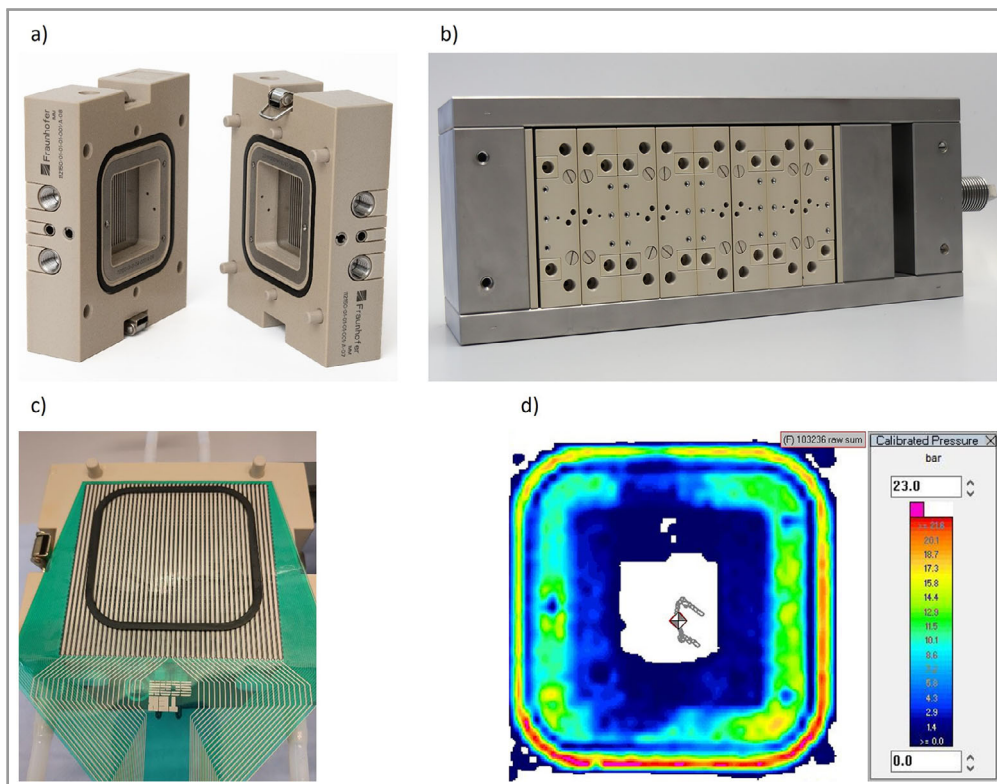


Figure 2. (a) Open flow cell without electrodes or separators. (b) Mechanical press with four flow cells. (c) Force field measurement: flow cell with black EPDM gasket, electrode area 5 cm², I-Scan[®] measurement foil. (d) Force field measurement: color scale in bar, EPDM gasket is visible as yellow-reddish outer ring. A torque of 30 Nm was applied to the mechanical press.

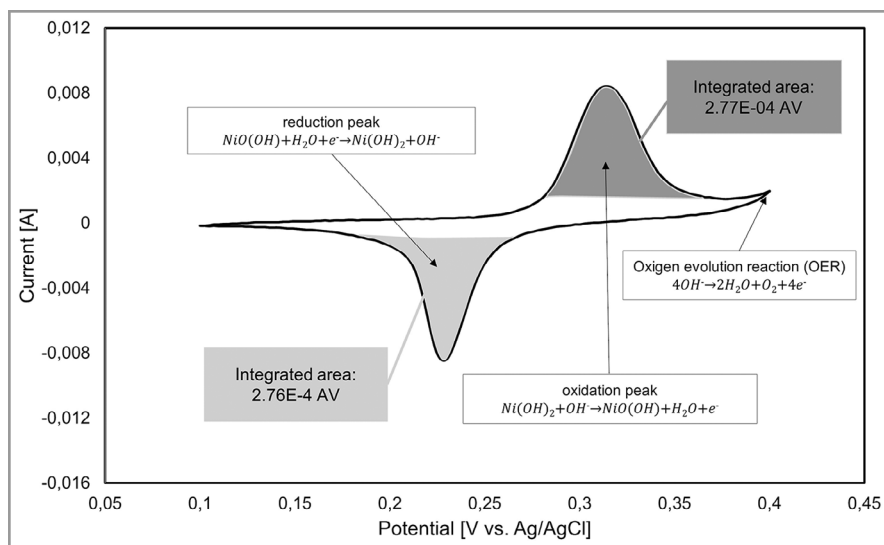


Figure 3. Cyclic voltammogram on the anode cell with reference electrode Ag/AgCl (3 M NaCl) connected by a Haber-Luggin capillary, scan rate (ν_{CV}) 20 mV s^{-1} , anolyte/catholyte (6 M KOH) with a flow of 20 mL min^{-1} .

can be adjusted, enabling different applications like experiments with a bulk electrolyte or zero-gap application such as proton exchange membrane (PEM) or anion exchange membrane (AEM) water electrolysis. The electrode area is adjustable in the range of 1 to 19 cm^2 . Furthermore, it is possible to implement a reference electrode. The sealing concept of the flow cells is an adapted concept for high-throughput screening and is aligned with the industrial standard for stacked flow cells. The aim of this screwless

design is to shorten the preparation time and to create a uniform contact pressure over all flow cells (Fig. 2b).

To measure the force field that is applied to the seal in the flow cell, an I-Scan[®] measurement was carried out by CMV Hoven GmbH in cooperation with TEKSCAN, Inc. (Figs. 2c and 2d). The I-Scan[®] measurement foil comprises a matrix of sensors and is placed between the half-cells, replacing the hte membrane during the measurement. Fig. 2d presents the first exemplary results for the local contact pressure on the EPDM gasket during optimization. The measurement shows that the applied pressure is distributed relatively homogeneously over the EPDM gasket.

4 Electrochemical Experiments Using the Newly Developed Flow Cell

Various established electrochemical experiments were carried out and evaluated to test the functionality of the flow cell. The cells were prepared for the alkaline water electrolysis (AWE) [10, 11] (Sect. 4.1, 4.2, and 4.3) and the alkaline water electrolysis with AEM as follows (Sect. 4.4) [12–14].

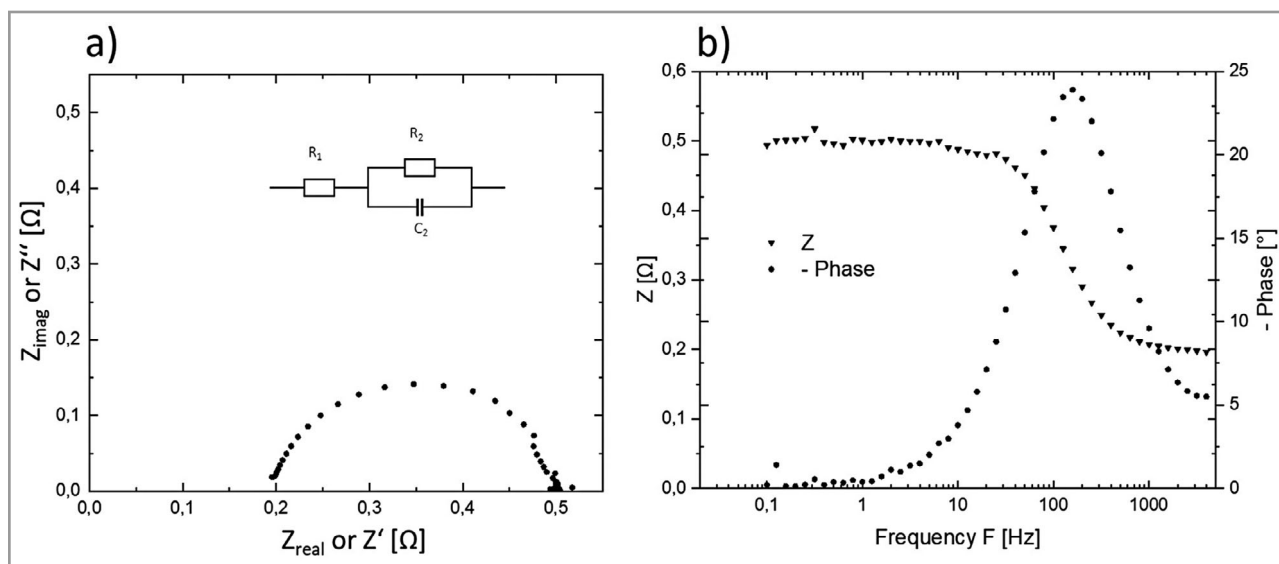


Figure 4. Nyquist plot including equivalent circuit model (a) and Bode plot (b), potential 0.5 V vs. Ag/AgCl, amplitude = 0.01 V, frequency range from 4 kHz to 0.1 Hz.

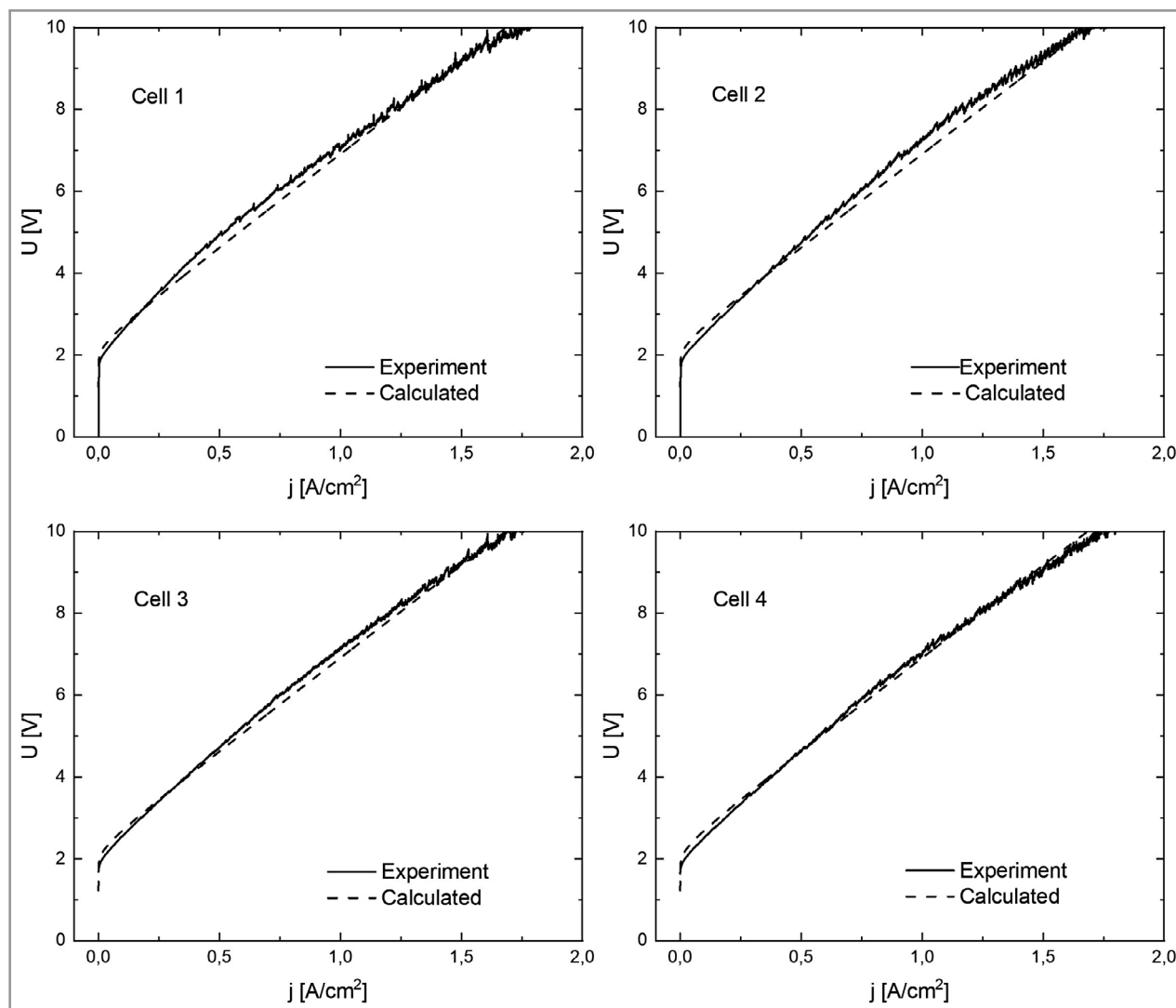


Figure 5. Comparability of the polarization diagrams of four flow cells for AWE in gap configuration in 6 M KOH as liquid electrolyte, scan rate: 5 mA s^{-1} , step-size: 0.002 A. The calculated curves correspond to theoretical Tafel plots with contributions from electrodes and electrolyte resistance. The resistance of the diaphragm can be neglected.

For the AWE tests, the cells had an electrolyte gap between the electrode and the membrane and were equipped with nickel foil ($127 \text{ }\mu\text{m}$, 99.83 %, Thermo Scientific Chemicals, cold-rolled sheet quality) 5 cm^2 as both anode and cathode, and a Zirfon® 220 μm thick diaphragm. The 6 M KOH electrolyte was prepared from 45 % KOH (extra pure, Carl Roth) and a cell pressure of 0.2 barg was applied at $20 \text{ }^\circ\text{C}$. Further, in some experiments, the cells were connected to a reference electrode (Ag/AgCl, 3 M NaCl) via a Haber-Luggin capillary at 5 mm distance from the anode, and the electrolyte flow was set to 40 mL min^{-1} (except Fig. 3).

For initial tests with AEMs, a setup in zero gap configuration was used with a sustainion® X37-50 membrane combined with an untreated Freudenberg H23C2 GDLs, as

anode and cathode, and the electrolyte was diluted to 1 M KOH.

4.1 Electrode Surface Roughness by Cyclic Voltammetry Measurements

The electrode surface roughness of nickel electrodes can be derived from cyclic voltammetry (CV) measurements. The results (Fig. 3) in the potential range between 0.1 V and 0.4 V vs. Ag/AgCl show the respective oxidation and reduction peaks for the Ni(II) and Ni(III) electrode surface as well as the onset potential for the oxygen evolution reaction [15–17]. The integrated areas of the reduction and the oxidation peaks are of similar values, as expected.

Table 1. Comparability of the polarization diagrams of four flow cells for AWE in 6 M KOH; exemplary data at three current densities, j [mA cm^{-2}].

Flow cell [V]	20 mA cm^{-2}	800 mA cm^{-2}	1400 mA cm^{-2}
1	2.014	6.231	8.775
2	1.993	6.289	8.917
3	2.030	6.243	8.711
4	2.003	6.175	8.742
RSD [%]	0.789	0.752	1.036

The surface charge of an electrode Q_{Ni} can be calculated from the reduction peak integral between the peak limits φ_o and φ_u in Fig. 3 to:

$$Q_{\text{Ni}} = \frac{1}{v_{\text{CV}}} \cdot \int_{\varphi_u}^{\varphi_o} I \cdot d\varphi_{\text{ME}} = \frac{1}{20 \cdot 10^{-3} \text{ V s}^{-1}} \cdot \int_{0.1\text{V}}^{0.27\text{V}} I \cdot d\varphi_{\text{ME}} = 1.38 \cdot 10^{-2} [\text{C}] \quad (1)$$

The roughness factor of the real nickel electrode can be calculated from the ratio of the real electrode area compared to the geometrical surface area in the cell using the specific charge of a polycrystalline nickel surface from literature [17] to:

$$f_R = \frac{A_{\text{active}}}{A_{\text{geometrical}}} = \frac{\frac{Q_{\text{Ni}}}{420 \cdot 10^{-6} \text{ C cm}^{-2}}}{5 \text{ cm}^2} = 6.60 [-] \quad (2)$$

This roughness is typical for cold-rolled non-porous metal surfaces with values from 1 to 10 [18].

4.2 Material Resistance and Interface Capacity

Potentiostatic electrical impedance spectroscopy (PEIS) was executed in a frequency range from 4 kHz to 0.1 Hz at a potential of 0.5 V vs. Ag/AgCl in a three-electrode configuration (Figs. 4a and 4b). The Nyquist plot shows one ohmic resistance corresponding to the electrolyte resistance ($R_1 = 0.19 \Omega$) and a combined ohmic/capacitive resistance corresponding to the electrode/electrolyte interface ($R_2 = 0.32 \Omega$), which are visualized in the equivalent circuit model.

From literature [19], a conductivity of $k = 0.5697 \text{ S cm}^{-1}$ for 6 M KOH at 20 °C is proposed. Hence, for the 5-mm electrolyte layer in the half cell (measured between Haber-Luggin

capillary and electrode) with a geometrical surface area of 5 cm^2 at 20 °C the resulting resistance would be:

$$R = \frac{L}{k \cdot A_E} = \frac{0.5 \text{ cm}}{0.5697 \text{ S cm}^{-1} \cdot 5 \text{ cm}^2} = 0.175 [\Omega] \quad (3)$$

The small deviation from the measured 0.19Ω could be due to slight temperature variations, electrolyte concentrations in the vicinity of the electrode or an electric resistance.

4.3 Comparability Measurements

A check for comparability was undertaken by simultaneously characterizing four similar cells using two-electrode configuration without reference electrode in a parallel setup. As shown in the polarization diagrams, when increasing the current density, the measured cell voltage immediately reaches roughly 2 V and then increases linearly (Fig. 5).

All cells showed good comparability with a maximum deviation of relative standard deviation (RSD) = 1.036 % (Tab. 1), which is within quality limits of reasonable comparability for high-throughput heterogeneous catalysis screening.

4.4 Membrane Stability Test

A stability experiment far above the typical single cell voltage of up to 10 V was performed in AEM zero gap configuration to check if such high voltages lead to short circuits or shunt currents.

While cells 2 and 3 survived these severe conditions outside the supplier specifications without a loss in reproducibility, cell 4 showed a deviation from the expected result after exceeding a potential of 2 V (see lower arrow in Fig. 6).

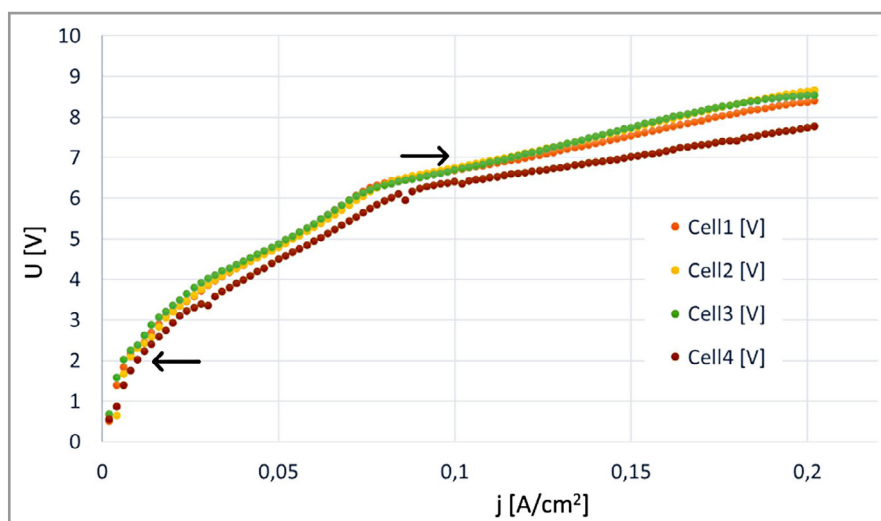


Figure 6. Polarization curves of four cells showing the effect of membrane stability in AEM electrolysis, 1 M KOH, flow 40 mL min^{-1} , 1 barg.

Later disassembly proved that the membrane of cell 4, and to a minor amount also that of cell 1 beyond 7 V (see upper arrow in Fig. 6), had defects and the graphite gas diffusion layer (GDL) was oxidized by the environment and electrochemical potential at the anode.

This test at unusually high voltage indicates how the stability of the membranes and electrodes can be evaluated and further proves the valid electrical sealing concept at 1 barg.

5 Conclusion

The developed parallel setup chosen in the experiments allowed for a direct comparison. Some learnings from these experiments with four parallel cells can be summarized as follows:

- Comparability of polarization diagrams in a parallel setup shows deviations of the voltage between the cells of <1 % RSD.
- CV measurement with the cell reveals electrode surface roughness on Ni as anticipated in the literature.
- Impedance measurement allows for conductivity evaluation of the electrolyte.
- I-Scan[®] measurement demonstrates that the applied pressure on the cell is distributed relatively homogeneously.
- Test performed using AEM in zero-gap cell configuration allows evaluation of membrane and electrode stability and reveals valid electrical sealing concept.

The proposed high-throughput approach provided initial results of improved reproducibility and will accelerate electrochemical screening as shown in alkaline water electrolysis for hydrogen production. Later, this approach will be used for other applications, e.g., in the field of organic electrochemistry. Standardized electrochemical flow cells, electrochemical analyzers, fully integrated software, and reliable conditioning protocols seem to be key requirements of these systems.

Acknowledgment

Part of this work received funding from the German Federal Ministry of Education and Research (Bundesministerium für Bildung und Forschung, BMBF) under grant no. 03SF0627A “iNEW2.0-Inkubator Nachhaltige Elektrochemische Wertschöpfungsketten”.

Abbreviations

AEM	anion exchange membrane
AWE	alkaline water electrolysis
CV	cyclic voltammetry
EIS	electrochemical impedance spectroscopy

GC	gas chromatography
GDE	gas diffusion electrode
GDL	gas diffusion layer
LSV	linear sweep voltammetry
PEEK	polyether ether ketone
PEIS	potentiostatic electrical impedance spectroscopy
PEM	polymer exchange membrane or proton exchange membrane
RSD	relative standard deviation

References

- [1] U. Rodemerck, M. Baerns, in *Basic Principles in Applied Catalysis* (Ed: M. Baerns), Springer, Berlin **2004**. DOI: https://doi.org/10.1007/978-3-662-05981-4_7
- [2] P. Strasser, S. Gorer, Q. Fan, K. Chondroudis, K. Cendak, D. Giaquinta, M. Devenney, in *High-Throughput Screening in Chemical Catalysis* (Eds: A. Hagemeyer, P. Strasser, A. F. Volpe), Wiley VCH, Weinheim **2004**.
- [3] P. P. Pescarmona, J. C. Van Der Waal, I. E. Maxwell, T. Maschmeyer, *Catal. Lett.* **1999**, 63, 1–11.
- [4] J. Pérez-Ramírez, R. J. Berger, G. Mul, F. Kapteijn, J. A. Moulijn, *Catal. Today* **2000**, 60 (1), 93–109. DOI: [https://doi.org/10.1016/S0920-5861\(00\)00321-7](https://doi.org/10.1016/S0920-5861(00)00321-7)
- [5] A. Müller, S. Coenen, M. Dejmek, D. Dogan, R.-A. Eichel, F. Eversheim, J. Fechtmann, S. Haug, B. Hecker, C. Hofmann, C. Hose, F. Huber, Fr. Huber, H. Kost, C. Kröger, P. Löb, O. Püttmann, F. Schneider, H. Tempel, G. Wasserschaft, D. Zahlmann, A. Ziogas, *DGMK Conf. Proc.* **2022**, 3, 104–121.
- [6] E. Brightman, J. Dodwell, N. Van Dijk, G. Hinds, *Electrochem. Commun.* **2015**, 52, 1–4. DOI: <https://doi.org/10.1016/j.elecom.2015.01.005>
- [7] M. Schalenbach, O. Kasian, K. J. J. Mayrhofer, *Int. J. Hydrogen Energy* **2018**, 43 (27), 11932–11938. DOI: <https://doi.org/10.1016/j.ijhydene.2018.04.219>
- [8] M. Quentmeier, B. Schmid, H. Tempel, H. Kungl, R. A. Eichel, *ACS Sustainable Chem. Eng.* **2023**, 11 (2), 679–688. DOI: <https://doi.org/10.1021/acssuschemeng.2c05539>
- [9] E. Robens, B. Hecker, H. Kungl, H. Tempel, R. A. Eichel, *ACS Appl. Energy Mater.* **2023**, 6 (14), 7571–7577. DOI: <https://doi.org/10.1021/acsaem.3c00985>
- [10] S. Marini, P. Salvi, P. Nelli, R. Pesenti, M. Villa, M. Berrettoni, G. Zangari, Y. Kiros, *Electrochim. Acta* **2012**, 82, 384–391. DOI: <https://doi.org/10.1016/j.electacta.2012.05.011>
- [11] K. Zeng, D. Zhang, *Prog. Energy Combust. Sci.* **2010**, 36 (3), 307–326. DOI: <https://doi.org/10.1016/j.peccs.2009.11.002>
- [12] Z. Liu, S. D. Sajjad, Y. Gao, H. Yang, J. J. Kaczur, R. I. Masel, *Int. J. Hydrogen Energy* **2017**, 42 (50), 29661–29665. DOI: <https://doi.org/10.1016/j.ijhydene.2017.10.050>
- [13] P. Fortin, T. Khoza, X. Cao, S. Y. Martinsen, A. Oyarce Barnett, S. Holdcroft, *J. Power Sources* **2020**, 451, 227814. DOI: <https://doi.org/10.1016/j.jpowsour.2020.227814>
- [14] H. A. Miller, K. Bouzek, J. Hnat, S. Loos, C. I. Bernäcker, T. Weißgärber, L. Röntzsch, J. Meier-Haack, *Sustainable Energy Fuels* **2020**, 4 (5), 2114–2133. DOI: <https://doi.org/10.1039/c9se01240k>
- [15] X. Li, F. C. Walsh, D. Pletcher, *Phys. Chem. Chem. Phys.* **2011**, 13 (3), 1162–1167. DOI: <https://doi.org/10.1039/c0cp00993h>

- [16] S. Klaus, Y. Cai, M. W. Louie, L. Trotochaud, A. T. Bell, *J. Phys. Chem. C* **2015**, *119* (13), 7243–7254. DOI: <https://doi.org/10.1021/acs.jpcc.5b00105>
- [17] M. E. G. Lyons, M. P. Brandon, *J. Electroanal. Chem.* **2010**, *641* (1–2), 119–130. DOI: <https://doi.org/10.1016/j.jelechem.2009.11.024>
- [18] V. M. Schmidt, *Elektrochemische Verfahrenstechnik: Grundlagen, Reaktionstechnik, Prozessoptimierung*, Wiley-VCH, Weinheim **2012**.
- [19] J. Rodríguez, S. Palmas, M. Sánchez-Molina, E. Amores, L. Mais, R. Campana, *Membranes* **2019**, *9* (10), 129. DOI: <https://doi.org/10.3390/membranes9100129>